Research Article

Janusz P. Kogut* and Elżbieta Pilecka

Application of the terrestrial laser scanner in the monitoring of earth structures

https://doi.org/10.1515/geo-2020-0033
received June 14, 2019; accepted February 6, 2020

Abstract: Terrestrial laser scanning (TLS) assists in the detection of the unsafe behaviour of slopes and scarps. It also facilitates the assessment of the stability of earthworks. Earth structures are those that are usually made of qualified ground material. One may distinguish between point structures such as mounds, forts and dams, and linear structures such as roads, railways and flood embankments. This article concerns the problem of monitoring and analysing of the effects associated with the unstable behaviour of selected earth structures. TLS enables remote sensing of surface changes in a simple and automated manner. Regular, multiple measurements with the laser scanner are applied in long-term monitoring of the behaviour of the selected objects. The discrete numerical models using, for example, the finite element method (FEM) take into account geotechnical properties of substrate and allow for the risk assessment and stability testing of such structures. The numerical model of the structure along with the parameters of the substrate are introduced into the FEM package. This allows for the analysis of stresses, strains and displacements, along with different loading cases. The work here presents a few selected earth structures for which the aforementioned analyses have been undertaken.

Keywords: laser scanning, slope stability, earth structures

1 Introduction

The purpose of monitoring areas threatened by soil mass movements is to determine the velocity and nature of the mass movements that cause terrain deformation. On the basis of repeated surveys, one may observe changes that have occurred within the analysed area, assess the likelihood of further development of the threat and establish ideas and opportunities for securing the endangered terrain. The landslides on which stability works have already been performed should also be monitored to assess the effectiveness of the methods applied. Among the different monitoring methods, there are two basic distinguishable groups – surface [1,2] and in-depth methods [3,4]. In order for monitoring results to be accurate and reflect the true situation as precisely as possible, the method of conducting the measurements should be selected appropriately. This stipulates that the measuring points be positioned properly and the effective analysis of the results obtained. Surface methods are designed to determine the deformations that occur on the surface of the terrain that are the direct cause of damage. Among them, one may distinguish between surveys, thanks to which it is possible to accurately find the displacements of specific measurement points and remote sensing methods. This allows for measurements without having to interfere with the tested ground. These can include air and terrestrial laser scanning (TLS) or satellite interferometry synthetic aperture radar (InSAR) [5,6]. Monitoring by means of surveying methods consists of taking repetitive geodetic measurements of the grid of measurement points that have been previously stabilised in the studied area. It is important to choose the location of measurement points – they should be located in areas where activity is the greatest. However, it is important to also set benchmarks outside the area exposed to movements, which will be the reference points in conducting measurements. The location of measuring points should be of long duration, in order to allow for multiple and reliable measurements. Applying the geodetic methods, it is possible to determine the range of active mass movements and their direction. It is also possible to estimate the size of the moving soil masses. Measurements can be used to determine changes within a certain time frame in the studied area, which are expressed by deformation indices such as depression, inclination,

* **Corresponding author: Janusz P. Kogut,** Cracow University of Technology, Civil Engineering Department, Warszawska 24, 31-155, Kraków, Poland, e-mail: jkogut@pk.edu.pl
Elżbieta Pilecka: Cracow University of Technology, Civil Engineering Department, Warszawska 24, 31-155, Kraków, Poland, e-mail: epilecka@pk.edu.pl

Open Access. © 2020 Janusz P. Kogut and Elżbieta Pilecka, published by De Gruyter. This work is licensed under the Creative Commons Attribution 4.0 Public License.

horizontal displacement, deformation or curvature. Measurements performed by means of laser scanning are one of the methods of remote sensing [7]. Remote sensing is a type of research performed from a distance – remotely and without contact – using specialised devices (sensors).

Remote sensing methods may be simply divided into active and passive. In active remote sensing, the impulse is sent from the device; and after reflection from the object, it is acquired and analysed. Active radar is an example of active remote sensing, during which microwaves are sent. Additionally, other examples include light detection and ranging (LiDAR), during which a light beam is sent, or sonar (sodar), where acoustic waves are sent [8]. Passive methods of remote sensing are those based on the analysis of signals emitted by the observed object. Photogrammetry is an example of passive remote sensing. It may be combined with the results of unmanned aerial vehicle surveys [9]. On the other hand, discrete numerical models using the finite element method (FEM) packages that take into account the properties of substrate, allow for risk assessment and stability of earth structures. The numerical modelling of the structure along with the parameters of the substrate also provides the analysis of stresses, strains and displacements for the consideration of different loading cases. This article presents a few selected earth structures, on which such mechanical analyses have been carried out. Nowadays, similar papers are published, which synthesise the results of geodetic surveys with discrete elements methods modelling [10,11]. Artificial intelligence methods are also employed as tools for soil stability assessment [12,13].

2 Methodology

2.1 Laser scanning and other surface measurements

Employing specialised software based on a cloud of points obtained from measurements using a laser scanner, it is possible to create a 3D terrain model after the processing of measurements. With the overlap of two or more modes made at time intervals, a differential model can be created, on the basis of which one may follow the process of deformation over time. The advantage of laser scanning lies in the fact that this measurement does not interfere with the tested environment. One may distinguish two types of laser scanning – airborne and terrestrial. Airborne scanning is carried out using the LiDAR system. The scanner is placed flat under an aeroplane fuselage. During the flight, a rectangular strip of land is registered, which lies in a plane transverse to the direction of flight. On the basis of the measurement of the return time sent from the signal scanner, which is reflected from the terrain surface, the distance between the plane and particular point of the terrain is determined. In airborne measurement using a laser scanner, a global positioning system or the global navigation satellite system determines the position of the pulse sending aircraft. The inertial navigation system defines the angular inclinations, in addition to the vectors of the platform acceleration on which the optical scanning head is mounted. This system measures the height coordinate with an accuracy of 15 cm. It allows the obtainment from one measurement of an image with an area of several square kilometres [5,7]. Another type of terrain observation that may be conducted is the use of a synthetic aperture radar (SAR) system. It consists of a satellite-based radar and a land-based processor. The radar sends microwave radiation towards the Earth's surface. After reaching the surface of the area, the radiation interacts with it, whereby it undergoes reflection, transmission or absorption. For each pixel of the radar picture, the SAR system registers the amplitude and phase of the reflected signal. It consists of a radar on board of satellite and a processor located on land. The radar sends microwave radiation towards the Earth's surface. After reaching the surface of the area, the radiation interacts with it (undergoes reflection, transmission or absorption). For each pixel of the radar picture, the SAR system registers the amplitude and phase of the reflected signal [6,7]. The InSAR method involves the processing of images that were made with one SAR antenna during subsequent satellite flights over the same area. For each pixel, the phase differences from two SAR images are calculated. On this posture, one gets an image of phase differences, which is called an interferogram. It consists of interference fringes that give information about the relative elevation of the land surface and its changes over time. This method allows remote, non-contact measurement with very high precision and frequency.

The TLS is another modern terrain mapping method. The measurements are based on the recording of a laser beam transformed later to the Cartesian coordinates. Usually, the TLS is placed on a geodetic tripod. In order to obtain greater accuracy of measurements to cover the scanning of larger areas, as well as to supplement areas that were in the shadow of previously scanned objects, terrestrial laser scanner measurements are performed from many positions. Each of these positions adjoins a common reference point. The data set (in the form of a cloud of points) creates an image of the

scanned space. The data measured are then archived for further processing. The difficulty in the laser recording process is the vast amount of data. Therefore, in the essential area being observed, data from various measurements are combined. The removal of additional objects (such as trees, shrubs, fences, etc.) is necessary and influences the simplicity of the scanned relief of the area. The measurements can be taken in the long scan mode, which is characterised by a maximum resolution. As a part of the surveying, a local situation and altitude map is made afterwards. The laser scanning process is based on automatic measurement of objects or terrain characterised by a very high sampling rate (3-D spatial measurement) of tens or even hundreds of thousands of points per second in real time. TLS used in this research has a high-speed data acquisition mode with up to several thousand measurements per second. As a result of the measurements, one may obtain a quasi-continuous mapping of the surrounding space represented by points. Each of these points has specific Cartesian coordinates (x, y and z) and are additionally enriched with intensity. The latter is another parameter (in the colour form), which results from different intensities of the measurement signal reflected from the scanned surface and depends on the type, colour and roughness of the tapping material. Additionally, an analogue or digital camera, with red–green–blue components of the measured objects may record data. Later on, in the post-processing, additional coloured textures reflecting the actual colours of the object may be obtained.

The file built as a result of scanning points is referred to as a "cloud of points," the number of which can reach up to many millions, whereby creating at the out-set a visualisation of the objects measured. The cloud of points is a kind of spatial documentation that one may return to at any time to perform further measurements or analysis. It also allows one to recollect the state of the day the scan has been performed. The accuracy of laser scanner measurements initially depends – similarly as in electronic tachymeters – on the accuracy of distance measurement and determination of angles. The quality of the results obtained also consists of other factors, such as the ability of the surface to reflect the laser beam as well as the impact of weather conditions such as scanner glare in strong sunlight, low temperature, dense fog or rainfall. In extreme case, these obstacles may prevent measurements completely or cause their delay. The assumed and even warp in the form of reference points is also affected by the quality of the final product. So is, to a very large extent, the process of combining point clouds from different measurement stations by the scans registered. An important parameter of scanners is the resolving power (the minimum distance between the measured points) and the size of the area, the diameter of which increases with distance.

This is due to the divergent nature of the laser beam. The resolving power of the RIEGL VZ-400, which is used in this study, is about 5 mm. Time resolution for the TLS depends on the task and is selected by the user. A high laser pulse repetition rate is up to 1.2 MHz, while the high-speed data acquisition mode is performed with up to 5,00,000 measurements per second and comes with a field of view from 100° to over 360°. The TLS has a range of measurements up to 800 m, with 5 mm accuracy and a precision of measurements about 3 mm [14]. The ordinates are determined using a method of direct survey in the field of the local coordinate system.

2.2 In-depth methods

The in-depth tests may be carried out using intrusive methods such as down-hole methods, especially in boreholes located at various depths in which measuring instruments are mounted. The results may provide information on the landslide activity by determining the size of dislocations on the surface and in-depth (inclinometers) as well as on the level of groundwater and water pore-pressure (piezometers). They are usually used when measuring unprotected landslides or to check the effectiveness of the performed protection works [2]. On the basis of data from inclinometer measurements, data on the depth, size, displacement velocities and the direction of deformation of the substrate are obtained. Thanks to these results, it is possible to determine the shape of the slip curve, the knowledge of which is the basis for designing the protection of the landslide. After installing the inclinometer, a zero measurement should be performed, also called a reference measurement, to which the results obtained in subsequent measurement sessions should be related. During inclinometer measurements, the slope of the probe is measured in relation to the vertical axis. Measurements are made by lowering and removing the probe from the inclinometer column. The first measurement is made at the bottom of the hole, then the probe is raised by a specific unit measuring section (generally 0.5 m) and reads until the probe is on the surface. A disadvantage of inclinometers is the short time of their use due to the fact that the landslides can quickly damage them. Extensometers are used for measuring soil compression, settlement and heave of soil and rock in tunnels, shafts and foundations as well as ground movement in boreholes. For example, the continuous rod

extensometer system accurately measures settlement and/or heave at single or multiple anchor points in a borehole and at its reference head, while incremental extensometer systems utilise electromagnetic induction phenomenon and together with inclinometer casing facilitates highly accurate measurements of ground movements in the direction of the borehole axis. Such system is capable of measuring movements as small as 0.001 mm with an accuracy of ±0.01 mm per meter. Piezometers are used to measure changes in the level of groundwater table or to measure the pore pressure of water in the subsoil. High-precision measurements can be made using commercially available piezometers with advanced measurement technology. Geophysical methods complement intrusive approaches, which sample only a very small proportion of the subsurface. They also complement walk-over or remotely sensed data, which principally provides information only at the ground surface. Advances in geophysical instrumentation, data processing, modelling and interpretation in the context of landslide monitoring are significantly improving the characterisation of hill slope hydrology. They are also improving the understanding of soil and rock hydrology and strength and their dynamics over time [4,15,16].

2.3 Landslide stability assessment

As it is commonly known, mass movements may have a strong impact on the landscape, including building structures. They are regarded as natural disasters, and their consequences threaten the lives and health of people. They also lead to the damage of property. Nowadays the number of landslide areas that are used for the land development is growing. Geological and engineering conditions in the areas designated for future investment are often not accurately recognised, which in the case of the later activation of a landslide may have disastrous consequences. The landslide problem is particularly evident in transportation and infrastructure engineering [17,18]. As a result of unfavourable climatic conditions, such as frequent torrential rains and flooding, active landslides may destroy the existing communication routes. Therefore, securing an active landslide in such an area often requires a large amount of work and investment. Landslides may occur when earth structures are built either in inadequate or in weak soil conditions, or with the use of poorly built-in soil. The stabilisation of landslides aims at ensuring an increase in slope stability, and properly made protection should eliminate the causes of the threat.

2.4 Discrete methods of the slope stability analysis

The results of the slope stability may be strongly influenced by the calculation method. Nowadays computational techniques based on analytical and numerical methods are applied. The analytical methods include the methods of Felleniuss [19], Bishop [20], Morgenstern-Price [21], Sarma [22] among others. There are only applied to the plane strain conditions. The numerical methods are based on approximation algorithms, where the landslide area is divided into a finite number of discrete elements. The FEM is based on the discretisation of a physical model [23,24]. In the FEM, the continuum is replaced by an equivalent discrete model. The calculation method used in this study is based on shear strength reduction method (SRM). This is a non-linear method of the limit equilibrium theory [25]. The SRM analyses the minimum safety factors and failure behaviours using various shapes, loads and initial boundary conditions. The SRM may be used to simulate the failure process without any previous assumptions and may be applied either to the plane or to the spatial deformation state. The method gradually decreases the cohesion and internal friction angle until the computation process does not converge. Hence, the obtained point is considered to be the failure point of the slope. The iteration starts with a limit state equilibrium that is subsequently incremented. With the updates of factor of safety (FOS), the cohesion and internal friction angle are scaled down. The maximum shear strength reduction (SSR) ratio at that point is used to calculate the minimum safety factor. Stability by SRM is achieved by weakening the soil in an elasto-plastic discrete analysis until the slope fails. The FOS is considered as the factor by which the soil strength is to be reduced to reach failure [25].

3 Road embankment under the landslide conditions

3.1 Problem formulation

A frequently used method of road surface diagnostics in landslide areas is the use of reference marks and inclinometers to assess the rate of deformation growth in the analysed area. Diagnostics of existing structures

are based on surveying and the results of numerical analysis [21]. They can be effectively applied to structures and can enable the assessment of the current state of the structure in emergency or anomalous situations. The measured values of vertical deformations of reference marks make it possible to determine the approximate surface deformation of the area, which in the case of comparison with the results obtained in numerical packages is associated with some errors. Linear infrastructure facilities, which include road embankments, are often characterised by the lack of fixed points enabling quick assessment of the structural failure. Hence, the diagnostics are established on both the numerical modelling results combined with the ground response. The ground response is usually evaluated by different measurement techniques. The assessment of compliance of the numerically obtained settlements with the measurement results makes it possible to evaluate the data for further numerical modelling. It also contributes to the determination of the deformation growth in the analysed road cross section, which is located on the active landslide. Numerical analysis along with the processing of data obtained by means of TLS has been developed and described in this research. The analysis uses vertical displacements of the road surface located on the active landslide. The geotechnical engineering parameters from the documentation [26] and the level of the water table measured by piezometers have been used. They are based on static calculations, due to the assumed analysis time corresponding to the implementation of neighbouring ground measurements with laser scanning. On the basis of slope stability analysis, it is that the road embankment was located along an active landslide. The road embankment described here was located on a quaternary layer of anthropogenic soil (layer formed from a mix of concrete crumbles, pebbles and gravels up to a thickness of 3.0 m). In addition to this, soft sandy clays were present in the bottom part of the layer I. In layer I at a depth of between 1.6 and 3.5 and 6.2 m below the ground surface, water filtration was found. Furthermore, below layer I there were quaternary soil columns of clay and sandy–silty clay, in addition to clay with sandstones and shales. Layer II was characterised by a variety of cohesive soil from firm to soft plastic. The bottom of layer II was located at a depth of 17 m below the ground surface. Layer II covers the entire area examined. The thickness of that layer is approximately equal to 25 m. The last layer is identified as the Upper Cretaceous, which has already been damaged by soil mass movement as well as flysch formation (layer III), which includes clay shales, shales and fine-grained sandstones. Layer III is also located in the entire area below layer II. Figure 1 presents the overview of the road embankment located along the slope. One may notice significant deformations of the topsoil and visible damage of the road subgrade.

Figure 1: The overview of the road embankment located along the slope.

3.2 Deformation monitoring

Monitoring with the use of TLS enabled the generation of a quasi-continuous mapping of the scanned area in the form of a cloud of points located in space by means of Cartesian coordinates. Comparison of the spatial models obtained led to the observation in differences of deformations that had occurred between two consecutive measurements. The location of the road embankment on the active landslide had led to the necessity of covering the road cross section with regular terrestrial monitoring. Terrain deformation measurements enabled the calibration of the numerical model, along with material data and substrate parameters. These measurements of TLS were carried out in the time interval. The first measurements were carried out for over 6 months. The measurements were performed using TLS located along the landslide analysed. Figure 2 displays the surface of the terrain and the road embankment represented by the cloud of points. Based on two consecutive measurements, a numerical differential model was built. Figure 3 presents such a differential model. From Figure 3, it is noticeable that the vertical deformations are up to 50 cm. It is clearly indicated that the road is located on the terrain of an active landslide.

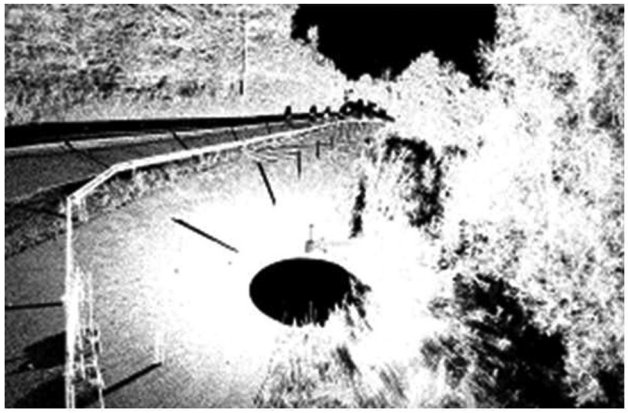

Figure 2: The surface of the road embankment represented by the cloud of points [27].

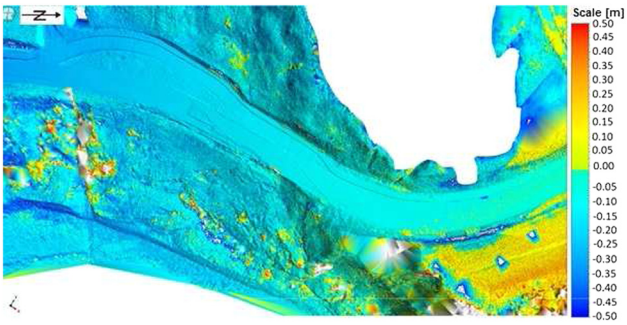

Figure 3: A differential model of the road embankment located along the slope [27].

3.3 Numerical model of the road embankment

TLS monitoring was carried out in late autumn and early spring. Based on a cloud of points measured, a 3D terrain surface was generated from the approximation of the point cloud using the finite elements technique. Following this, the spatial analysis of the road embankment was then made using the FEM package MIDAS GTS NX [28]. The numerical model was built taking into account the relief of the terrain surface obtained on the basis of TLS. The soil surface and the spatial arrangement of geotechnical layers, as well as the ground-water table, were modelled using data from geotechnical profiles taken from four different boreholes. The approximation of geotechnical layers was carried out with the assumption of a linear change along the boreholes. The numerical model utilised 13,95,941 hexahedral finite elements creating 2,44,102 nodes and 7,32,306 degrees of freedom (Figure 4). The number of equations was equal to 7,16,030. The boundary conditions were sliding joints with respect to the vertical axis, with blocking

Figure 4: 3-D model of the terrain implemented into the FEM package MIDAS GTS NX.

displacements in the horizontal direction, for the planes *xz* and *yz*. The bottom of the model was fixed along the *x*, *y* and *z* axes. The values of the effective internal friction angle φ' and cohesion c', soil unit weght γ' and the liquidity index I_L were adopted according to the existing documentation, while the Young moduli E_0 and Poisson ratio ν were adopted in accordance with the locally occurring parameters [26]. The clay layer was modelled as an elasto-plastic Coulomb–Mohr soil model. Both the shale layer and the road were modelled as isotropic elastic constitutive material. Table 1 presents the parameters used in further analysis.

The calculations were carried out in two steps. The first step included obtaining a spatial state of stress of the soil, corresponding to the condition prevailing on the day of the first measurement with TLS. The displacements and deformations of the model were omitted. The next step contained the model deformation analysis obtained after the time corresponding to the second TLS measurement. The analysis time was assumed to be 125 days. The model omitted the influence of the dynamic impact of passing vehicles on the propagation of deformations along the analysed landslide area. The numerical analyses performed so far [29] indicate that, the passage of vehicles at various speeds through the

Table 1: Parameters used in FEM model of the analysed road embankment [26]

Layer	φ' [deg]	c' [kPa]	Young modulus E_0 [MPa]	Poisson ratio ν [–]	Density ρ [G/CM^3]	I_L [–]
Clay (II)	6.75	25	9.1	0.3	1.956	0.80
Shales (III)	—	—	1,000	0.2	2.149	—
Embankment	—	—	3,000	0.3	2.5	—

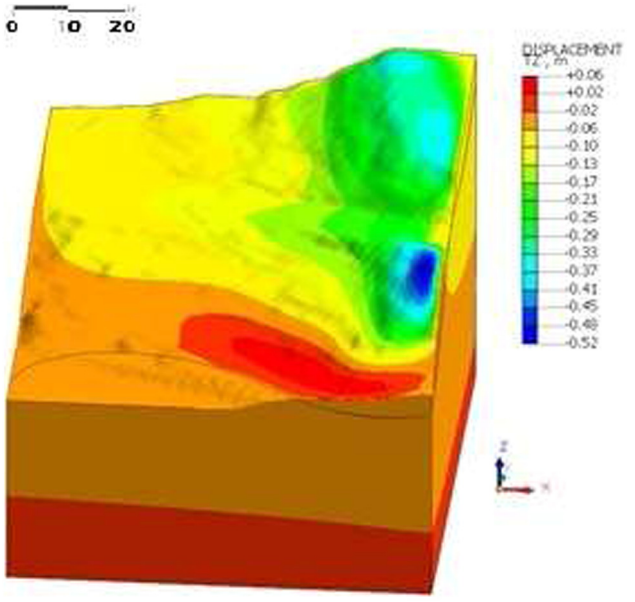

Figure 5: The vertical displacements of FEM model of the analysed road embankment.

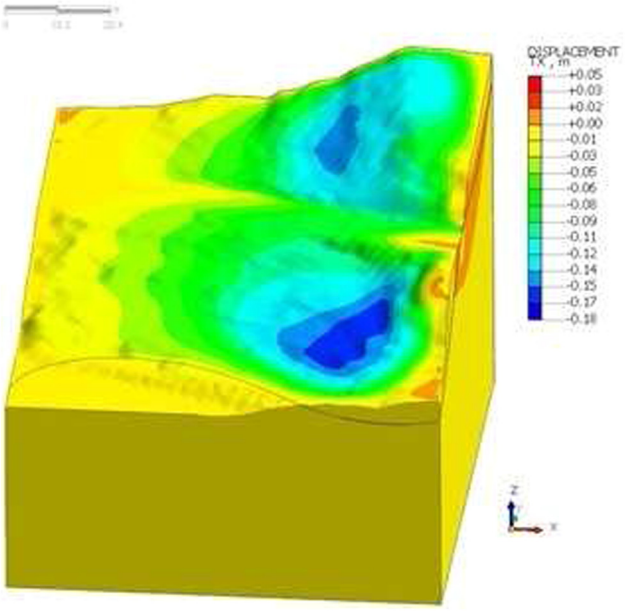

Figure 6: The horizontal displacements of FEM model of the analysed road embankment in the direction perpendicular to the existing road.

analysed landslide caused an increase in deformation in the initial stage only. This was manifested by a decrease in the landslide stability at the beginning. However, over a longer period of time the dynamic deformations became stable. Figure 5 presents vertical deformation of the analysed area. It is visible in the figure that there is an uplift in the lower part of the terrain, while the horizontal displacements shown in Figures 6 and 7 indicate lateral movement of the landslide has developed.

The comparison of the results obtained from the measurements displays dominant vertical displacements of between 5 and 20 cm located along the road curvature. There is an increase in the vertical deformations in the north-western part caused by repairs on the temporary surface of a concrete slab. Figure 3 shows the change in the provisional route of the road in comparison with the measurement of the area nearly a year earlier, in order to model the surface area. The differential model of vertical deformations clearly indicates the development of a landslide along the analysed road. The numerical results of the model indicate the predominant settlement in the range of 5–20 cm, similar to the results obtained from TLS.

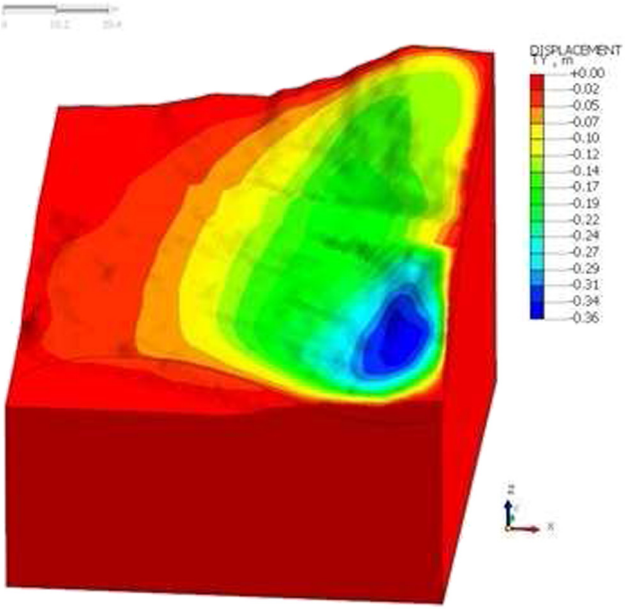

Figure 7: The horizontal displacements of FEM model of the analysed road embankment in the direction parallel to the existing road.

Here, too, attention should be paid to the significantly smaller vertical settlements obtained in the northern part of the numerical model in comparison with the corresponding terrain obtained from the TLS. This is due to the inclusion in the numerical analysis of the area of land relief obtained from the first measurements, which did not include the construction of a temporary road. In Figures 6 and 7, the area which is threatened by the largest mass movements and where landslide activity is visible is clearly outlined. Increased horizontal displacements of up to 40 cm also dominate the arc of the analysed road section. This coincides with the observations of the road surface condition, on which in the considered section numerous transversal and longitudinal cracks were observed. Based on a previously performed series of analyses, it may be found that numerical modelling and surface TLS monitoring appropriately evaluated the behaviour of road and its vicinity. The assessment of the usefulness of a road embankment may enable the estimation of the exploitation time of a given road section. This is due to the occurrence time of vertical displacements which cause significant damage or failure of the pavement. It may also support decision makers on the repair of, or complete road shutdown from traffic at risk of structural failure.

4 A route with the noise barrier and the retaining wall

4.1 Problem formulation

This section presents the results of TLS of the soil–structure interaction in the Carpathian flysch conditions. It may help to evaluate the usefulness of the method for monitoring the deformations of the terrain over the potential slip surfaces. Flysch may be characterised by a particular susceptibility to mass movements, due to its geological structure. The Carpathian flysch is described in a simplified way as alternating layers of sandstone and clay shales [30–32]. It is in the layers of the clay shales that the slip surface may be activated due to the high susceptibility for shale to absorb water and soften. Another feature of the geological structure of the Carpathian flysch is the existence of a weathered rock layer beneath the soil surface. This is distinguished by a large gradation of rock material. Such a weathered layer of debris laid on the bedrock also has a high susceptibility to creating landslides, when the slip surface nucleates between the weathered material and the bedrock. The situation presented in this section focuses on forecasting a threat, especially during the current climate changes. It demands a detailed investigation of soil conditions to an appropriate level below the ground surface and the diagnosing of the occurrence of one or more potential slip surfaces. Quaternary deposits recognised here are composed of silty soils (such as silty clays and clays) on the layer of debris. Below this, sandstones and shales are present. The groundwater is found within the Quaternary aquifer. The groundwater table is variable, with an average value of 2.0 m below the ground surface level. A single-family dwelling house is located on the hill slope. It is considered to be an additional load on the site. In the vicinity of the slope, a dual expressway has been built, along with a noise barrier located within the traffic lane. Therefore, earthworks were carried out involving the removal of the overburden soil and the construction of the escarpment. Figure 8 presents the overview of the slope with the retaining structure and noise barriers located on the slope. The results of the analysis indicate the impact of the road excavations on the stability of the built-up slope. Numerical calculations of the dry slope performed so far showed that the slope stability factor with the excavation made is about 15% less than the slope stability factor without excavation. An additional existing destabilising factor may be the rise of the groundwater table. The groundwater reduces the stability by about 20% [34]. This means that an excavation of

Figure 8: Overview of the slope with retaining structure and the noise barriers [33].

the road and the raising of the groundwater level increases the threat to the road infrastructure. The Carpathian flysch is a difficult subgrade in road engineering due to its complicated structure and the landslide threat. Very often the first slip surface is located on the border of the weathered zone of the flysch and the rock, as it turned out to be in this particular case. The scarp presented here has failed due to the road excavation during the construction process in the complicated flysch conditions. Hence, the construction of a retaining structure has become crucial. It was built during a period of unfavourable weather conditions, including heavy rains.

4.2 Deformation monitoring

Figure 9 presents the differential model of the slope with the retaining structure and noise barriers. The displacements of the slope are visible only in the behaviour of the noise barriers. It seems to be stable with small vertical settlements around the retaining structure. The retaining structure measurements are not credible, regarding the fact that the aggregate has been disintegrating due to the weathering processes. The comparison of the results of the TLS measurements shows dominant vertical displacements of the noise barrier in the range from −2 to +2 cm.

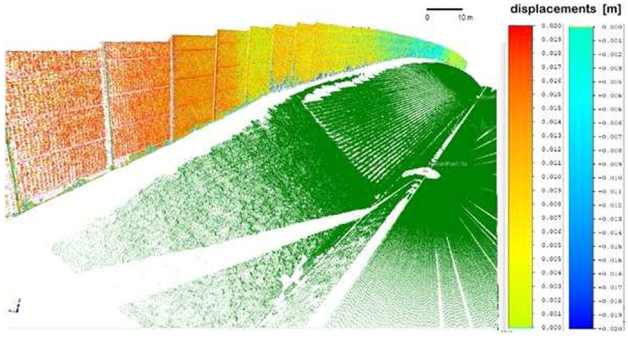

Figure 9: Differential model of the noise barriers [33].

4.3 Numerical model of the slope

There was the requirement for the proper prediction of the behaviour of the structures in the vicinity of the road cross section. It was required to build a numerical model and analyse long-lasting effects. Also, in this case the values of the effective internal friction angle φ' and cohesion c', soil unit weght γ' and the liquidity index I_L were adopted according to the existing documentation [35]. Additionally, the deformation moduli E_0 and Poisson ratio ν were adopted in accordance with the locally occurring parameters. Table 2 presents parameters used in the analysis. The clay layers are modelled as elasto-plastic Coulomb–Mohr soil models. Both shale layers are modelled as isotropic elastic constitutive material. The analysis has been performed using the FEM package MIDAS GTS NX. The numerical model utilised 4,49,430 hexahedral finite elements creating 82,575 nodes and 2,47,725 degrees of freedom. The number of equations was equal to 2,40,384. In Figure 10, the mesh of FEM numerical model of the slope is visible, with the retaining structure and noise barriers. The total displacements of the noise barriers located on the slope are similar to those registered by the TLS. They reach about 4 cm. Figure 11 presents the vertical deformations of the terrain with analysed structures, while Figure 12 presents the horizontal deformations obtained from the numerical model in the direction perpendicular to the existing highway. Figure 12 displays displacements of the retaining structure and top of the soil up to 2 cm in the direction of a road and the rotation of the noise barrier.

This section presents the results of TLS measurements in the Carpathian flysch conditions, which may help to evaluate the usefulness of the monitoring methods for the deformation on the terrain surface over the potential slip surfaces. The measurement results, taken from the site and carried out over several months, indicated the possible existence of a local landslide threat even after stabilisation works. However, the deformations found were rather small and could not be dangerous for the nearby road infrastructure. The results obtained displayed the usefulness of TLS to

Table 2: Parameters used in FEM model [35]

Layer	φ' [deg]	c' [kPa]	Young modulus E_0 [MPa]	Poisson ratio ν [−]	Density ρ [G/CM^3]	I_L [−]
Shales (Ia)	—	—	1,000	0.2	2.158	—
Clay (Ib)	12	20	12.5	0.25	1.991	0.29
silty clay (Ic)	8	10	10	0.25	1.838	0.42
Shales (II)	—	—	3,000	0.2	2.256	—

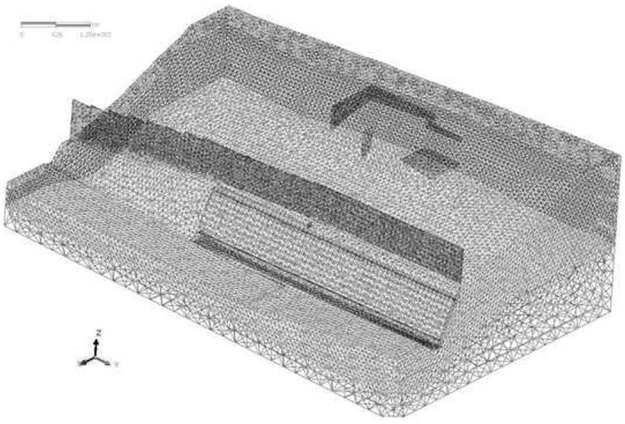

Figure 10: FEM mesh of the slope with retaining structure and the noise barriers.

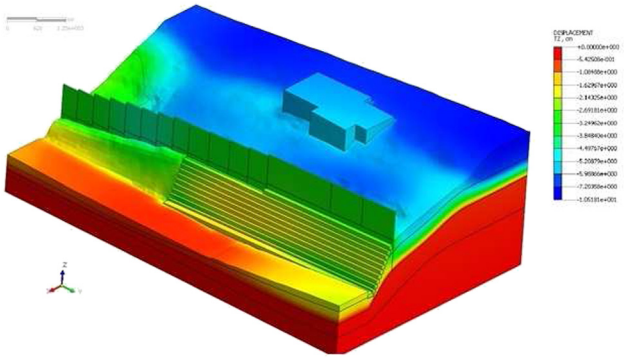

Figure 11: The vertical displacements of FEM model of the slope with retaining structure and the noise barriers.

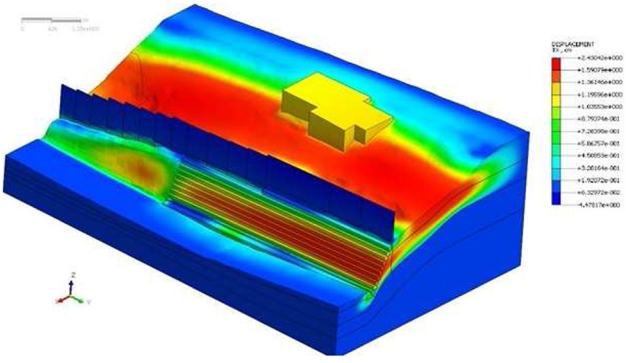

Figure 12: The horizontal displacements of FEM model of the slope with retaining structure and the noise barriers.

recognise discontinuous deformations of the terrain surface in such harsh soil conditions. They are a starting point in the discrete analyses of slope stability as visible in the case analysed here illustrated by the FEM results. The results may be used to assess the causes of potential damage to structures associated with landslide activity.

5 Historical Kościuszko mound stability problem

5.1 Geology and hydrogeological conditions of the mound

The Kościuszko mound was built between 1,820 and 23 and is an anthropogenic soil mound dedicated to commemorate the Polish and American national hero. The steep sloping angle of the mound varies from 46° to 51° (at its base). The area where the Kościuszko mound is located is within the tectonic framework of the Wolski Forest and St. Bronisława Hill. The latter is the largest and the highest raised log element in the area of Krakow and was created during the tectonic movements in the Miocene. It is almost entirely covered with Quaternary deposit, except for the Jurassic limestones. Boreholes made in the mound area have illustrated that the limestones underneath the embankment are weathered, strongly fractured and affected by the karst process. Loess cover of the hill appeared during the North Polish glaciation period. Loess sediments occur in the form of silts (Si), clayey silts (clSi) and sandy silts (saSi) and often contain admixtures of limestone crumbs. The Kościuszko mound is located in the basin of the Rudawa river, a left-bank tributary of the Vistula, which flows 750 m north-east of the mound. The Vistula River currently flows 1.1 km to the south-east of the mound, and 2 km to the south-east is the Zakrzówek Reservoir, which is the closest water reservoir to the mound [36]. The groundwater is found within the Quaternary and Jurassic aquifer. The groundwater of the quaternary floor is mainly related to the filtration within the loess formations. Depending on the intensity of precipitation, variations in the water depth are considerable. Water in loess formations occurs locally. The Jurassic groundwater is associated with limestones cut with faults that are cracked and partially karst. Within the Kościuszko mound, there is a low level of groundwater.

However, it is possible that there is gravitational groundwater. It can occur in silt deposits in the form of a filter, the intensity of which may vary depending on the depth. In periods of prolonged rainfall or spring thaw, groundwater of high intensity may be found at small depths. The landslide on Kościuszko mound covered an area of about 0.25 ha and almost the entire oval cone. The mass movements and subsidence almost cover the entire body of the Kościuszko mound, except the small part in the northern part. They are occurring from an altitude of 329 m above sea level at the top to 295 m

above sea level at the bottom of the cone in the eastern part of the mound. The research conducted has shown that the material being moved is anthropogenic soil, which is formed in the form of cohesive soils, in particular silt and clayey silt. The embankment is set on a thin layer of quaternary native soils (with a thickness of less than 4 m) that lie on Jurassic limestones. The roof of limestone rocks is inclined towards the east, which also affects the directions of deformation. The movement of earth masses occurring in this area is a rotational slip combined with creeping and flowing. The landslide processes on the Kościuszko mound have taken place nearly continuously from the moment of erection. There have been much damage, especially after long rainfall (the documents mention dates between 1,830 and 1,840), but the largest damage took place after the rains in 1997 and 2010. The year 1997 was the turning point for the Kościuszko mound because of the long-lasting heavy rains. As a result, a landslide had been activated, and cracks made it possible for water to penetrate inside the mound. The concrete paths were completely destroyed, and the platform bent in a north-west direction, threatening to topple the commemorative boulder on top of the mound into the chapel. The mound began to fall apart from the top, breaking in half – the state of the mound was a disaster. In 2000–2002, the renovation of the Kościuszko mound was completed. The top of the cone was reconstructed by dismantling a delaminated 9-m section of the embankment. Over the surface of the slope, injection bolts were installed and the surface was secured with geomats. An high-density polyethylene (HDPE) membrane was placed on the exposed part. The embankment was rebuilt from soil which had been mixed with soil from the dismantling of its central part and a gravel mix with geo-grid reinforcement in the outer part. In 2002–2003, the depth and surface monitoring networks were set up using inclinometers and piezometers. Several works including drainage systems, foil protection, geo-membranes, micro-piles and soil anchors have been undertaken year after year. However, they might have been ineffective. This may have been due to the inadequate geological survey. All of the tests only included the surface layer of the embankment (down to a depth of 4.5 m), whereby deeper layers of soil that built the mound and native soils and rocks were not recognised accurately. Up until the last occurrence of a Kościuszko mound landslide, which occurred in May 2010 due to the heavy rain period, nearly 50% of the mound's surface had been destroyed. Temporary safeguards in the form of geo-grids, ropes and anchors were installed and slowed the flow process but did not ensure the stability of the cone. Since then, the technical condition of the mound is considered bad. Several tests carried out in 2012, presented in geo-engineering documentation, constitute a detailed recognition of the ground of the Kościuszko mound. Substrate research showed high variability and heterogeneity of soils that build the mound's body, and their sensitivity to changes due to the water content and consistency. The upper part of the mound embankment was rebuilt during renovation in 2002. Additionally, a small embankment with concreted paths constructed during the renovation process in the area that remained intact are made of non-cohesive soils such as medium sands (MSa), gravely sands (grSa), silty sands (siSa), gravely silty sands (gr-siSa) and silty sandy gravels (sisaGr). These soils occur in medium dense and loose condition. The remaining part of the embankment, which was intact during renovation, was separated from the upper part by a waterproof HDPE membrane. It is made of cohesive soils of silts (Si), clayey silts (clSi), sandy silty clays (sasiCl) and clayey sandy silts (clsaSi). There are also occasional crumbs and pebbles. The soil is characterised by variable water content and various consistency ranging from stiff to soft. Soil is firm, but then plastic, and the least in the soft plastic state. In the central part of the embankment, as well as in the western, south-eastern and south-western section, low water content soils are consolidated. However, farther from the central axis of the cone the proportion of soils in a firm state decreases, whereby the southern section is comprised of medium to soft state plastic soils. There is no quaternary water table in the area subjected to analysis. After careful elaboration of the documentation [37], it may be pointed out that the causes of landslide processes in this area may be due to geological structure, because the mound lump is an anthropogenic soil, mostly silt and silty clays, which tend to settle under the loading. These soils are sensitive to water changes and show a serious decrease in strength parameters. Moreover, the steep slope of the mound leads to the penetration of water from precipitation and thaws into the embankment. It also leads to the water content growth of the mound soil caused by the poor drainage system and improper protection of the mound's body.

5.2 Deformation monitoring

The measurements of the area of the Kościuszko mound were made by a terrestrial laser scanner. Figure 13

Figure 13: The aerial view of the mound with points of the TLS location.

presents the overview of the mound with several points of the TLS location marked. The measurements were performed over a year apart. Figure 14 presents the surface of the mound represented by the cloud of points. By overlapping two clouds of points representing the same surface, it was possible to create a differential model, which showed that almost the whole mound had deformed over the year between the measurements.

Figure 14: The surface of the mound represented by the cloud of points.

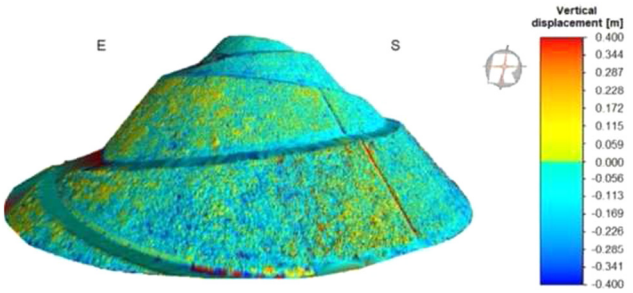

Figure 15: Differential model of mound as viewed from the west [1].

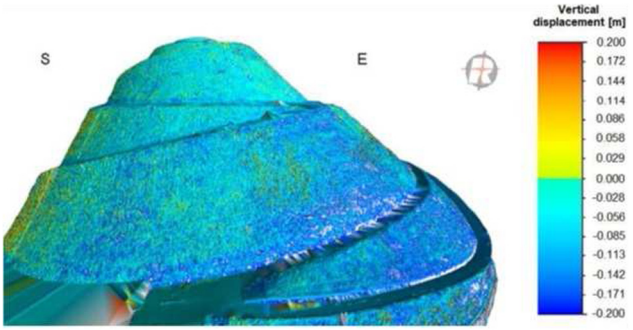

Figure 16: Differential model of mound as viewed from the south [1].

Figure 15 displays a differential model of the mound viewed from the west, while Figure 16 presents a differential model of the mound viewed from the south. The slope is mainly deformed on the eastern side, which is sliding (displacement differences range from –40 to +40 cm), while the bottom part of the slope is deformed in general. On the south-eastern side, the largest displacements (–20 cm) occur near the lowest walking path and over the existing retaining walls. Slope increments on the southern side are on average 5 cm, and in the lower part they vary from –20 cm locally to +13 cm. Large deformations may be observed near the drainage system where displacements reach up to +20 cm. The north-eastern, north and west sides are dominated by displacement increments of 10 cm. The part of the mound below the top of the observation platform is the least deformed, where local surface displacements only occur in the northern section (within 8 cm). Slope displacements increase as you approach the base of the embankment.

5.3 Stability analysis of the Kościuszko mound

In order to determine the stability of the Kościuszko mound, numerical modelling was carried out. A cross

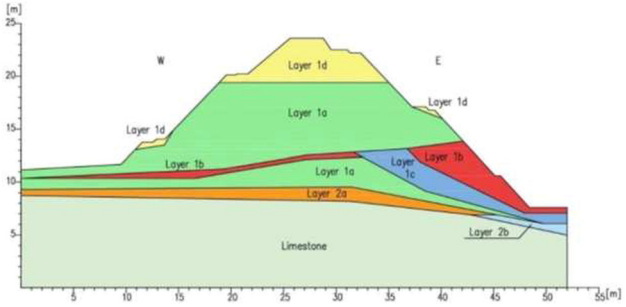

Figure 17: A cross section of the mound with the layers of soil applied to the numerical model [1].

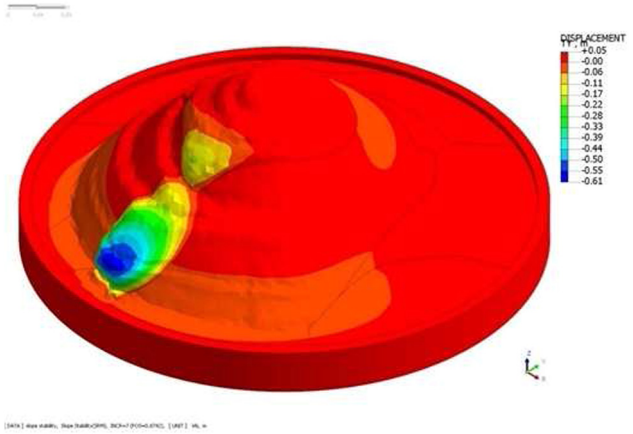

Figure 18: The horizontal displacements of FEM model of the mound in the *Y* direction of local frame of reference.

section on the east-west line (Figure 17) was selected here to show variations in the soil. It was selected on the basis of the results of TLS measurements, covering the most deformed areas. The stability of the Kościuszko mound was checked using an MIDAS program. The numerical analysis was carried out using an SSR technique. The Coulomb–Mohr model was adopted to illustrate the behaviour of the anthropogenic layers, and the elastic model for the limestone layer found in the base. The basic loading was the own weight of the mound. The geometry of the model and the soil conditions (Table 3) were selected on the basis of the results of geological surveys [1]. The width of the mound is 52 m and the height is 23.5 m (at the highest point). The layers marked 1a–1d consist of anthropogenic soil and layers 2a and 2b are original soils. The upper part of the mound is made of non-cohesive soils, namely, medium sand (MSa), medium sand with gravel (grSa), medium or fine sand with silt (siSa), sand with silt and gravel (sigrSa), gravel with sand and silt (sasiGr) and gravel with sand (saGr). The lower part of the embankment is made of cohesive soils, namely, silts (Si), silts with clay (clSi), clay with silts and sand (sisaCl), and silts with clay and sand (clsaSi). The whole earth structure is located on the limestone.

The results of the presented analysis refer to a situation with a critical stability. An analysis of slope stability with an MIDAS package demonstrates that the FOS is equal to 0.874. This value is smaller than the critical state value when FOS = 1.00. Therefore, it is necessary to control the development of soil movements in this area. The process of slope destruction has started in the lower part of the slope and proceeds towards the top on the eastern side. The slip surface is clearly developed (Figure 18). The most serious damage to the slopes is in the lower part of the mound and decrease towards its top. The vertical displacements visible in Figure 19 indicate that the platform located on the top of the mound would settle up to 40 cm, while the lower part uplifts and moves creating a niche. The area covered by the occurrence of landslide movements and the direction of their development obtained on the basis of the analysis coincides with the results of monitoring by TLS. Earth structures such as Kościuszko mound, which originated from anthropogenic soils, confirm that their analysis ought to be based on both detailed recognition of geological and engineering conditions occurring in the landslide area and further TLS. Such an analysis of mound destruction is much more effective. Mound monitoring using TLS has made it possible to create a

Table 3: Parameters used in FEM model [1]

Layer	φ' [deg]	c' [kPa]	Young modulus E_0 [MPa]	Poisson ratio v [–]	Density ρ [G/CM^3]	I_L [–]
1a	24	33	30.2	0.08	2.149	—
1b	20	29	30.7	0.12	2.094	—
1c	14	20	9.55	0.23	2.013	—
1d	30	—	28	0.25	1.96	—
2a	25	32	29.2	0.08	2.123	—
2b	18	30	20.7	0.12	2.088	—
Limestone	—	—	7,445	0.25	2.3	—

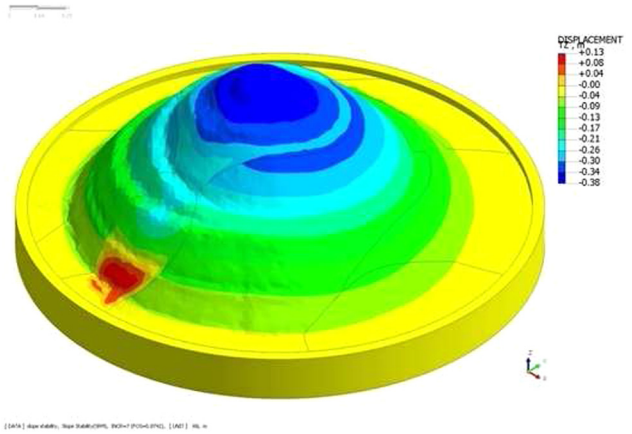

Figure 19: The vertical displacements of FEM model of the mound.

differential terrain model. Moreover, it has helped to assess the development of the landslide process and determine the most deformed areas and the range of the displacements. Furthermore, the analysis has shown the most likely slip surface in the same location, where the largest deformations of the mound were observed. Similar analysis has been done using Plaxis 3-D package [38]. Although the soil of the mound was precisely modelled, and the FOS was greater than the critical state value, but in the opinion of this paper's authors the displacements in analysed cases were too large.

Nowadays, the mound priority is to temporarily secure or repair damage that threatens the stability of slopes. One may specify that among the works requiring immediate intervention include the protection of cracked walking paths, repair of the drainage system, the filling of hollows and the protection of balustrades surrounding the observation platform on the top the mound. The FOS is smaller than the critical value and further degradation of the earth structure means loss of stability. This study has presented results therefore, which may serve as a basis for a project to secure against such landslide.

6 Discussion

The problems of landslide phenomena occurring in earthworks described above are still the matters of importance. The modern computing environment allows advanced analysis of this type of phenomena with increasing precision and accuracy. Moreover, the use of modern devices for surface displacement measurement allows for more accurate mapping of the terrain, while the use of wide range of experimental methods allows for more accurate mapping of the subsoil. This permits the construction of complex numerical models that help to analyse the behaviour of earth structures and predict their stability. In all three cases analysed above, laser surface scanning allowed to build spatial models with high accuracy. The use of FEM, in turn, allowed for a more accurate analysis of the substrate, which is usually performed as a 2-D problem. Currently, the numerical capabilities associated with the increased performance of computers, their operational memory and computational capabilities yield much more efficient and effective solving and analysing such spatial 3-D cases checking the stability of the subsoil and earth structures, and the possibility of their protection against the loss of stability. The next step will be the construction of systems that permit online monitoring and analysis of such structures, which will take place in real time and protect against negative effects the propagation of landslide processes in advance.

7 Conclusions

Based on the performed series of analyses, it can be concluded that the numerical modelling and the surface monitoring by laser scanning technology may be successfully utilised for diagnostic evaluation of the state of earth structures. Through estimating the time of occurrence of displacements which cause significant damage or failure of the structure, it may be possible to find the optimal time to safely service, or simply make a decision on the repair of structural damage. The measurement results, taken from the site may indicate the possible existence of the local landslide threat before, during and even after stabilisation works. The results obtained illustrate the usefulness of applying TLS to recognise discontinuous deformations of the terrain surface in complicated soil conditions. They might be a starting point in the discrete analyses of the stability of earth structures, as in examples of those analysed here which were illustrated by the FEM results. The results may be used to assess the causes of potential damage to structures associated with landslide activity. Mound monitoring using TLS demonstrated that it is possible to build a reliable differential terrain model. Further implementation and development of FEM models may help to assess the progress of landslide processes as well as to determine predominant deformed areas and the range of the deformations.

References

[1] Pilecka E, Tomaszkiewicz K. Stability analysis of the Kościuszko mound using terrestrial laser scanner and numerical modelling. E3S Web Conf. 2018;66(01018):1–9.

[2] Skrzypczak I, Kokoszka W, Zientek D, Kogut J. Monitoring of landslide areas with the use of contemporary methods of measuring and mapping. Civil Environ Eng Rep. 2017;24(1):69–82.
[3] Intrieri E, Gigli G, Casagli N, Nadim F. Brief communication. Landslide early warning system: toolbox and general concepts. Nat Hazards Earth Syst Sci. 2013;13:85–90.
[4] Whiteley JS, Chambers JE, Uhlemann S, Wilkinson PB, Kendall JM. Geophysical monitoring of moisture-induced landslides: a review. Rev Geo-Phys. 2019;57:106–45.
[5] Ferretti A. Satellite InSAR Data: reservoir monitoring from space (EET 9). European Association of Geoscientists and Engineers EAGE; 2014.
[6] Hannsen RF. Radar interferometry. Data interpretation and error analysis. Heidelberg: Springer Verlag; 2005.
[7] Fujii T, Fukuchi T, editors. Laser remote sensing. Taylor & Francis, CRC Press; 2005.
[8] Frehlich RG. Estimation of velocity error for Doppler lidar measurements. J Atmos Ocean Technol. 2001;19:355–66.
[9] Barlow J, Gilham J, Ibarra-Cofra I. Kinematic analysis of sea cliff stability using UAV photogrammetry. Int J Remote Sens. 2017;38(8–10):2464–79.
[10] Ossowski R, Tysiąc P. A new approach of coastal cliff monitoring using mobile laser scanning. Pol Marit Res. 2018;25(2):140–7.
[11] Tysiąc P, Wojtowicz A, Szulwic J. Coastal cliffs monitoring and prediction of displacements using terrestial laser scanning. Baltic Geodetic Congress (Geomatics). Gdańsk, Poland; 2018.
[12] Atkinson PM, Tatnall A. Introduction neural networks in remote sensing. Int J Remote Sens. 1997;18:699–709.
[13] Lee S, Ryu JH, Won JS, Park HJ. Determination and application of the weights for landslide susceptibility mapping using an artificial neural network. Eng Geol. 2004;71:289–302.
[14] Riegl TLS Field Operation Manual and Workflow. Boulder, Co: UNAVCO; 2013.
[15] Harba P, Pilecki Z. Assessment of time-spatial changes of shear wave velocities of flysch formation prone to mass movements by seismic interferometry with use of ambient noise. Landslide. 2017;14:1225–33.
[16] Pilecki Z. Basic principles for the identification of land-slides using geophysical methods. E3S Web Conf. 2017;24(01001):1–8.
[17] Kaczmarczyk R, Tchórzewska S, Woźniak H. Description of selected landslides from southern Poland activated after intensive rainfall in 2010 (in Polish). Biul Państwowego Instytutu Geologicznego. 2011;446(1):65–73.
[18] Kogut JP, Pilecka E, Szwarkowski D. Analysis of landslide effects along a road located in the Carpathian flysch. Open Geosci. 2018;10:517–31.
[19] Fellenius W. Calculation of the stability of earth dams. Transactions. 2nd Congress on Large Dams. Vol. 4. Washington, DC; 1936. p. 445–63.
[20] Bishop AW. The use of the slip cirlce in th stability analysis of slopes. Géotechnique. 1955;5(1):7–17.
[21] Morgenstern N, Price V. The analysis of the stability of general slip surfaces. Géotechnique. 1965;15(1):79–93.
[22] Sarma S. Seismic stability of earth dams and embankments. Géotechnique. 1975;25(4):743–61.
[23] Bathe KJ. Finite element procedures in engineering analysis. Englewood Cliffs, New Jersey: Prentice-Hall; 1982.
[24] Zienkiewicz OC, Taylor R. The finite element method for solid and structural mechanics. Amsterdam, Boston: Elsevier Butterworth–Heinemann; 2005.
[25] Griffiths D, Lane P. Slope stability analysis by finite elements. Géotechnique. 1999;49(3):387–403.
[26] Dokumentacja geologiczno-inżynierska dla stabilizacji os-uwiska w ciągu DW 981 odcinek 100 km 3 + 890 – 3 + 980 w miejscowości Kąclowa, Q-5583. Tech. rep., Kraków; 2015.
[27] Pilecka E, Szwarkowski D. Diagnostyka nasypu dro-gowego zlokalizowanego na czynnym osuwisku z wykorzys-taniem naziemnego skaningu laserowego i numerycznego modelowania. Autobusy. 2016;12:382–6.
[28] Manual specifications. Midas GTS NX; 2016.
[29] Pilecka E, Szwarkowski D, Manterys T. Wpływ drgań drogowych na propagację deformacji wzdłuż czynnej powierzchni poślizgu i stateczność nasypów na terenach osuwiskowych. Autobusy. 2016;6:394–402.
[30] Alexandrowicz Z, Margielewski W. Impact of mass movements on geo – and biodiversity in the Polish Outer (Flysch) Carpathians. Geomorphology. 2010;123:290–304.
[31] Jastrzębska M, Łupieżowiec M. Analysis of the causes and effects of landslides in the Carpathian flysch in the area of Milówka and evaluation of their prevention methods. Ann Wars Univ Life Sci. 2018;50(2):195–211.
[32] Margielewski W. Structural control and types of movements of rock mass in anisotropic rocks: case studies in the Polish Flysch Carpathians. Geomorphology. 2006;77:47–68.
[33] Kogut JP, Tymoshenko I. Remote sensing of Carpathian flysch landslides with the use of terrestrial laser scanner. E3S Web Conf. 2018;66(01019):1–10.
[34] Pilecka E, Kogut JP. Soil mass movements as threats to the road transportation infrastructure. TTS, Technika Transportu Szynowego Koleje, Tramwaje, Metro. 2015;12:2825–30.
[35] Faron K, Kos J, Szymonik L. Ekspertyza tech-niczna konstrukcji oporowej skarpy wykopu drogi ekspresowej S69 w km 5 + 500 jezdni lewej w Bielsku-Białej i urządzeń odpowiedzialnych za odwodnienie terenu skarpy wykopu Q-5629. Tech. rep., Kraków; 2016.
[36] Wójcik R, editor. Kopiec Kościuszki i jego położenie geologiczne: atlas – przewodnik. Kraków: Urząd Miasta Krakowa, Wydział Kształtowania Środowiska; 2016.
[37] *Dokumentacja geologiczno-inżynierska dla rozpoznania podłoża, dla potrzeb opracowania zabezpieczenia obiektu stożka Kopca Kościuszki wraz z otoczeniem, zniszczonego przez aktywne osuwisko*. Tech. rep., Kraków; 2013.
[38] Wrana B, Pietrzak N. Slope stability estimation of the Kościuszko Mound in Cracow. Studia Geotechnica et Mechanica. 2015;37(2):93–101.